ELSEVIER

Chemical Engineering Journal 91 (2003) 181–189

Chemical Engineering Journal

www.elsevier.com/locate/cej

Mathematical modelling of exothermic catalytic reaction in a single partially-wetted porous catalyst particle

Irina A. Mikhailova [a,*], Valeri A. Kirillov [a], Stanislav I. Fadeev [b], Mikhail G. Slin'ko [c]

[a] *Boreskov Institute of Catalysis, 5 Pr. Lavrentieva, Novosibirsk 630090, Russia*
[b] *Sobolev Institute of Mathematics, Novosibirsk, Russia*
[c] *Karpov Institute of Physical Chemistry, Moscow, Russia*

Abstract

The mathematical model for the multiphase steady-state processes on a partially-wetted porous catalyst slab in the conditions of the exothermic catalytic reaction, species diffusion, phase transitions, and capillary phenomena interaction is developed. Numerical experiment was carried out for the model reaction of α-methylstyrene hydrogenation. The impact of the external wetting efficiency on the steady-state regimes of the slab is investigated. The partially-wetted regime is characterised by studying the width of the dry zone inside the slab; the slab overheating, the area of the multiplicity.

Keywords: Exothermic catalytic reaction; Partially-wetted porous catalyst; Steady-state processes

1. Introduction

Catalytic processes in multiphase reactors are often considered to be very prospective for industrial applications. This induces the particular attention to the study of multiphase catalytic reactions in a single particle level. Numerous experimental studies [1–3] report the multiplicity of catalyst particle steady states in a multiphase catalytic process. In recent research [4], multiplicity of α-methylstyrene hydrogenation was studied.

In literature, there are many models describing multiphase processes on a single catalyst particle under certain conditions and assumptions. In the experimental and theoretical studies [2,5,6], it was assumed that condensation may occur inside the particle, while the external surface of the catalyst particle is dry. Some models [7,8] considered the catalyst particle, which is partially-wetted on its external surface but is fully wetted inside due to the capillary forces. The latter approach may be applied to isothermal conditions but it does not suit modelling exothermic reactions with volatile components. The modelling a non-isothermal process in a half-wetted slab was developed in [9]. The assumption of a single pore size allowed the authors of [9] to consider the distribution of liquid and gas phases inside the particle as a set of distinct completely flooded and gas-filled zones. The impact of vaporisation and imbibition processes on the formation of the hot-spot zone inside the particle was shown.

These mathematical models and some others were described in details in the review [10]. It is pointed out there that, although the sufficient success in modelling multiphase processes on porous catalyst has been achieved, the more common case of exothermic reaction on catalyst partially-wetted both on its external and internal surfaces is to be developed.

Data reported in the cited papers evidence the following:

(i) the catalyst particle can be either dry, filled with liquid (wetted) or partially-wetted, as well;
(ii) phase transitions (vaporisation and condensation) inside the catalyst particle can be very intensive;
(iii) impact of the capillary forces is significant to cause the imbibition of the liquid phase into the porous structure of the catalyst particle.

These three statements seem to be important and ought to be considered when making the numerical experiments.

We have recently developed the mathematical model for the "liquid–gas–solid" stationary catalytic process on the porous catalyst particle [11]. The main objective of the current research is the numerical study of the multiphase processes on a partially-wetted porous catalyst particle in the conditions of the exothermic catalytic reaction, species diffusion, phase transitions, and capillary phenomena interaction.

* Corresponding author. Tel.: +7-383-2341187; fax: +7-383-2341187.
E-mail address: v.a.kirillov@catalysis.nsk.su (I.A. Mikhailova).

1385-8947/02/$ – see front matter
PII: S1385-8947(02)00152-3

Nomenclature

A_i	coefficient in the expression for evaporation rate
b_G, b_L	dimensionless activation energy of the reaction
B_0	permeability of gas pores (m^2)
C_i	liquid phase weight fraction
C_i^*	liquid phase molar fraction
C_p	heat capacity ($J\,kg^{-1}\,K^{-1}$)
D_{ij}	binary diffusion coefficient ($m^2\,s^{-1}$)
D_{ik}	Knudsen diffusion coefficient ($m^2\,s^{-1}$)
D_L	effective diffusion coefficient in liquid phase ($m^2\,s^{-1}$)
E	activation energy of the catalytic reaction ($J\,kmol^{-1}$)
H_i	evaporation heat ($J\,kg^{-1}$)
k	kinetic constant of the reaction
k_0	pre-exponential factor in the Arrenius law
l	intraparticle position (m)
L	catalyst particle size (m)
m_i	order of the reaction
M_i	molar weight of a compound ($kg\,kmol^{-1}$)
N_i	gas phase flow ($kmol\,m^{-2}\,s^{-1}$)
Nu	Nusselt number
P	pressure (Pa)
Pr	Prandtl number
q	coefficient in the expression for evaporation rate
Q	reaction heat ($J\,kmol^{-1}$)
Q_W	dimensionless reaction heat parameter
r	radius of a catalytic particle pore (m)
$\bar{r}$	average radius of catalytic particle pores (m)
$R = 8314$	the universal gas constant ($J\,kmol^{-1}\,K^{-1}$)
Re	Reynolds number
R_i	evaporation rate ($kmol\,m^{-3}\,s^{-1}$)
S	specific surface of the catalyst particle ($m^2\,kg^{-1}$)
Sc	Schmidt number
Sh	Sherwood number
S_{LG}	area of the liquid–gas interface ($m^2\,kg^{-1}$)
T	temperature (K)
u	imbibition velocity ($m\,s^{-1}$)
W	catalytic reaction rate ($kmol\,m^{-3}\,s^{-1}$)
x_i	gas phase molar fraction
z	co-ordination number
Z	effective heat of liquid evaporation

Greek letters

α	phase volume fraction
β_{ij}	mass-transfer coefficient ($m\,s^{-1}$)
β_T	heat-transfer coefficient ($W\,m^{-2}\,K^{-1}$)
ε	catalyst particle porosity
γ_L	permeability of liquid-filled pores ($m^2\,Pa^{-1}\,s^{-1}$)
Φ_M	dimensionless catalyst activity parameter
φ	wetting angle
λ	heat conductivity
μ	viscosity (Pa s)
ν	stoichiometric coefficient
θ	$(T - T_b)/b_G T_b$ dimensionless temperature
ρ	density ($kg\,m^{-3}$)
σ	surface tension at the liquid–gas interface ($J\,m^{-2}$)
τ	tortuosity of pores
$\xi = l/L$	dimensionless intraparticle position

Subscripts

b	reactor bulk
cat	catalyst particle
G	gas phase
$i, j = 1$–3	components: 1, H_2; 2, hydrocarbon reactant (α-methylstyrene); 3, hydrocarbon product (cumene)
L	liquid phase

2. Mathematical model

The mathematical model is based on the following main assumptions:

(1) Catalyst particle is a one-dimensional porous slab and distribution of pores by radii is given by a density function $f(r)$:

$$f(r) = \frac{r\exp(-r/\bar{r})}{(\bar{r})^2} \tag{1}$$

(2) The left side of the slab contacts with the liquid–gas film, the right side with the gas–vapor phase.

(3) All parameters and variables are considered for each value of intraparticle position, l, as average values for all elementary volumes in $(l; l+\mathrm{d}l)$. For each l, liquid-filled, $\alpha_L(l)$, and gas-filled, $\alpha_G(l)$, volume fractions are defined as follows:

$$\alpha_L(l) = \frac{\int_{r_{min}}^{r^*(l)} f(r)\,\mathrm{d}r}{\int_{r_{min}}^{r_{max}} f(r)\,\mathrm{d}r};$$
$$\alpha_G(l) = 1 - \alpha_L(l),\ r^*(l) \text{ is a critical pore radii} \tag{2}$$

(4) Both gas phase and liquid phase contain three components.

(5) Exothermic catalytic reaction of hydrogenation occurs in both gas and liquid phases.

(6) Rates of phase transitions are taken into account and are determined by the molecular-kinetic theory [12].

(7) Mass-transfer in liquid phase is submitted by effective diffusion and convective motion. It is taken into

account that gas phase contains components with sufficiently different binary diffusion coefficients. We use the Dusty Gas Model [13] for describing mass-transfer in gas phase.

(8) Temperature is equal for the co-existing phases in every point of the slab; heat transfer is performed by thermal conductivity (including gas, liquid and particle thermal conductivity) and convective motion of liquid and gas.

(9) Boundary conditions include: (i) mass-transfer in gas phase deduced from the Stefan–Maxwell equations [14] at both sides of the slab; (ii) heat-transfer at both sides of the slab; (iii) mass-transfer in liquid phase at the left side; (iv) the fixed value of external wetting efficiency at the left side. It is assumed that the bulk gas and bulk liquid are in equilibrium at the left side of the slab.

The mathematical model includes the overall equations of the mass balances in gas and liquid phases, correspondingly:

$$\frac{\mathrm{d}(\alpha_G N_i)}{\mathrm{d}l} = \nu_i W_G + R_i; \quad i = 1\text{–}3 \tag{3}$$

$$\frac{\mathrm{d}}{\mathrm{d}l}\left[D_L \alpha_L \rho_L \frac{\mathrm{d}C_i}{\mathrm{d}l}\right] - \frac{\mathrm{d}}{\mathrm{d}l}[u_L \alpha_L \rho_L C_i] + \nu_i M_i W_L - R_i M_i = 0; \quad i = 1\text{–}3 \tag{4}$$

The dusty gas flux relations are formulated as

$$\left(\frac{P_G}{RT}\right)\frac{\mathrm{d}x_i}{\mathrm{d}l} = \sum_{j=1, j\neq i}^{3} \frac{x_i N_j - x_j N_i}{D_{ij}^*} - \frac{N_i}{D_{ik}^*} - \frac{x_i}{RT}\left(\frac{B_0 P_G}{\mu_G D_{ik}^*} + 1\right)\frac{\mathrm{d}P_G}{\mathrm{d}l}; \quad i = 1\text{–}3 \tag{5}$$

$$\sum_{i=1}^{3} \frac{N_i}{D_{ik}^*} = -\frac{B_0 P_G}{RT\mu_G} \sum_{i=1}^{3} \frac{x_i}{D_{ik}^*} \frac{\mathrm{d}P_G}{\mathrm{d}l} \tag{6}$$

Here,

$$D_{ij}^* = D_{ij}\frac{\varepsilon}{\tau}, \quad D_{ij} = D_{ij}^0 \frac{P_G^0}{P_G}\left(\frac{T}{T_0}\right)^{1.7};$$

$$D_{ik}^* = \frac{2}{3}\frac{\varepsilon r_G}{\tau}\sqrt{\frac{8RT}{\pi M_i}}, \quad B_0 = \frac{\varepsilon (r_G)^2}{8\tau}$$

The Eq. (7) follows from (4), if $\sum_{i=1}^{3} C_i = 1$ and $\sum_{i=1}^{3} \nu_i M_i = 0$:

$$-\frac{\mathrm{d}}{\mathrm{d}l}[u_L \alpha_L \rho_L] = \sum_{i=1}^{3} R_i M_i \tag{7}$$

The Eq. (9) for the critical pore radius is derived from the Darcy's equation for liquid phase and the equation for the capillary pressure,

$$u_L = -\gamma_L\left(\frac{\mathrm{d}P_G}{\mathrm{d}l} - \frac{\mathrm{d}P_{cap}}{\mathrm{d}l}\right);$$

$$P_{cap} = \frac{2\sigma\cos\varphi}{r^*}, \ \gamma_L = \frac{\varepsilon}{8\tau\mu_L}(r_L)^2 \tag{8}$$

$$\frac{\mathrm{d}r^*}{\mathrm{d}l} = -\frac{u_L + \gamma_L(\mathrm{d}P_G/\mathrm{d}l)}{\gamma_L 2\sigma\cos\varphi/(r^*)^2} \tag{9}$$

The energy balance is presented by the Eq. (10):

$$\frac{\mathrm{d}}{\mathrm{d}l}\left[\lambda\frac{\mathrm{d}T}{\mathrm{d}l}\right] - \left[\sum_{i=1}^{3}\alpha_G N_i M_i C_{pGi} + u_L \alpha_L \rho_L C_{pL}\right]\frac{\mathrm{d}T}{\mathrm{d}l} + W_G Q_G + W_L Q_L - \sum_{i=2}^{3} R_i M_i H_i = 0 \tag{10}$$

Here,

$$\lambda = \varepsilon\alpha_G\lambda_G + \varepsilon\alpha_L\lambda_L + (1-\varepsilon)\lambda_{cat}$$

The reaction kinetic rates, W_G and W_L, in Eqs. (3), (4) and (10) are estimated as

$$W_G = k_G \alpha_G (P_G)^{m_1+m_2}(x_1)^{m_1}(x_2)^{m_2};$$

$$k_G = k_{0G}\exp\left(-\frac{E_G}{RT}\right) \tag{11}$$

$$W_L = k_L \alpha_L (C_1^*)^{m_1}(C_2^*)^{m_2}; \quad k_L = k_{0L}\exp\left(-\frac{E_L}{RT}\right) \tag{12}$$

The rates of the phase transitions depend on the internal liquid–gas surface, S_{LG}, adopted from [15], as well as on the difference between the current value of a mole fraction, x_i, and its equilibrium value, x_i^{eq}:

$$R_i = A_i \frac{q}{1-0.5q} P_G S_{LG} \rho_{cat} \sqrt{\frac{1}{M_i RT}}\left(x_i^{eq} - x_i\right) \tag{13}$$

$$x_i^{eq} = C_i^* \frac{P_i^0(T)}{P_G}\exp\left(-\frac{2\sigma V_i \cos\varphi}{RTr^*}\right) \tag{14}$$

$$S_{LG} = \frac{4\varepsilon S\alpha_L(1-\alpha_L^{z-1})}{\tau(z-2)(1-\varepsilon)(1+\sin\varphi)} \tag{15}$$

The model was completed by the boundary conditions described later.

At the left side of the slab ($l = 0$), Eqs. (16)–(20):

$$N_1 = \frac{P}{RT}\beta_{12}(x_{1b} - x_1) + \tilde{x}_1 \sum_{i=1}^{3} N_i \tag{16}$$

$$N_j = \frac{P}{RT}\beta_{12}\frac{(x_{jb} - x_j) + \tilde{x}_j(1 - (\beta_{12}/\beta_{23}))(x_{1b} - x_1)}{(\beta_{12}/\beta_{23}) + \tilde{x}_1(1 - (\beta_{12}/\beta_{23}))} + \tilde{x}_j \sum_{i=1}^{3} N_i; \quad j = 2, 3 \tag{17}$$

$$\lambda \frac{dT}{dl} = \left(\beta_T + \sum_{j=1}^{3} C_{p_{G_j}} M_i N_j \alpha_G + \alpha_L \rho_L u_L C_{p_L} \right) (T - T_b) \quad (18)$$

$$D_L \frac{dC_i}{dl} = (k + u_L)(C_i - C_{ib}); \quad i = 1\text{–}3 \quad (19)$$

$$P_G = P_{Gb}, \quad \alpha_L = \alpha_{Lb} \quad (20)$$

In Eqs. (16) and (17), $\tilde{x}_j$ corresponds to the concentration of species transferred by the Stephan flux within the boundary layer. In principle, $\tilde{x}_j$ lies between x_{jb} and $x_j|_{l=0}$, we considered $\tilde{x}_j = x_{jb}$. Mass-transfer coefficients β_{ij}, entering these formulas, are found from the traditional correlation for Sherwood number calculations (see, e.g. [16]):

$$\beta_{ij} = \frac{Sh_{ij} D_{ij}}{L}; \quad Sh_{ij} = 2 + 0.6 Re^{0.5} Sc_{ij}^{0.33},$$
$$Sc_{ij} = \frac{\mu_G}{\rho_G D_{ij}}, \ j = 2, 3, \ i \neq j \quad (21)$$

Heat exchange coefficient β_T is found from the correlation similar to (21):

$$\beta_T = \frac{Nu(\alpha_G \lambda_G + \alpha_L \lambda_L)}{L}; \quad Nu = 2 + 0.6 Re^{0.5} Pr^{0.33},$$
$$Pr = \frac{\mu_G \sum_{i=1}^{3} C_{p_{Gi}} x_i}{\rho_G (\alpha_G \lambda_G + \alpha_L \lambda_L)} \quad (22)$$

At the right side of the slab ($l = L$), Eqs. (23)–(27):

$$N_1 = \frac{P}{RT} \beta_{12} (x_1 - x_{1b}) + \tilde{x}_1 \sum_{i=1}^{3} N_i \quad (23)$$

$$N_j = \frac{P}{RT} \beta_{12} \frac{(x_j - x_{jb}) + \tilde{x}_j (1 - (\beta_{12}/\beta_{23}))(x_1 - x_{1b})}{(\beta_{12}/\beta_{23}) + \tilde{x}_1 (1 - (\beta_{12}/\beta_{23}))}$$
$$+ \tilde{x}_j \sum_{i=1}^{3} N_i; \quad j = 2, 3 \quad (24)$$

$$\lambda \frac{dT}{dl} = \left(\beta_T - \sum_{j=1}^{3} C_{p_{G_j}} M_i N_j \alpha_G - \alpha_L \rho_L u_L C_{p_L} \right) (T_b - T) \quad (25)$$

$$\frac{dC_i}{dl} = 0; \quad i = 1\text{–}3 \quad (26)$$

$$P_G = P_{Gb}; \quad \frac{d\alpha_L}{dl} = 0 \quad (27)$$

The detailed dimensionless description of this mathematical model is reported in [11]. The model parameters values corresponding to α-methylstyrene hydrogenation on a porous catalyst slab are provided in Table 1.

The non-linear model is solved using the original software package [17]. The procedure of the parameter continuation

Table 1
Parameter values used for the model result performance

Description	Parameters
Catalyst particle parameters	$L = 5 \times 10^{-3}$ m; $\bar{r} = 10^{-6}$ m; $S = 10^4$ m^2 kg^{-1}; $\varepsilon = 0.5$; $\tau = 1.5$; $\rho_{cat} = 1000$ kg m^{-3}; $\gamma_{cat} = 0.3$ W m^{-1} K^{-1}
Reaction conditions parameters	$P_{Gb} = 10^5$ Pa; $T_b = 405$ K; $x_{1b} = 0.6$; $x_{2b} = 0.4$; $C_{1b} = 0.4 \times 10^{-4}$; $C_{2b} = 1 - C_{1b}$; $Re = 100$
Chemical compounds data	$M_1 = 2$ kg kmol^{-1}; $M_2 = 118$ kg kmol^{-1}; $M_3 = 120$ kg kmol^{-1} $C_{pG1} = 14{,}425$ J kg^{-1} K^{-1}; $C_{pG2} = 1237$ J kg^{-1} K^{-1}; $C_{pG3} = 1271$ J kg^{-1} K^{-1} $\lambda_{G1} = 0.181$ W m^{-1} K^{-1}; $\lambda_{G2} = 0.019$ W m^{-1} K^{-1}; $\mu_G = 0.8 \times 10^{-5}$ Pa s $C_{pL} = 1780$ J kg^{-1} K^{-1}; $\lambda_L = 0.1$ W m^{-1} K^{-1}; $\mu_L = 0.74 \times 10^{-3}$ Pa s
Diffusion coefficients	$D_{12}^0 = 0.32 \times 10^{-4}$ m^2 s^{-1}; $D_{13}^0 = 0.32 \cdot 10^{-4}$ m^2 s^{-1}; $D_{23}^0 = 0.21 \times 10^{-5}$ m^2 s^{-1}; $D_L^0 = 0.9 \cdot 10^{-9}$ m^2 s^{-1}
Catalytic reaction parameters	$\nu_1 = \nu_2 = -\nu_3 = 1$; $b_G = \frac{RT_b}{E_G} = 0.08$; $b_L = \frac{RT_b}{E_L} = 0.05$ $Q_G = 1.09 \times 10^8$ J kmol^{-1}; $Q_L = 1.06 \times 10^8$ J kmol^{-1}
Phase transition parameters	$P_1^0 = 0.267 \times 10^9$ Pa; $P_2^0 = 131.57 \exp\left(16.45 - \frac{3644.30}{T - 64.65}\right)$ Pa; $P_3^0 = 131.57 \exp\left(15.92 - \frac{3363.6}{T - 63.37}\right)$ Pa $H_2 = 3.43 \times 10^5$ J kg^{-1}; $H_3 = 3.125 \times 10^5$ J kg^{-1} $\varphi = 60°$; $\sigma = 0.025$ J m^{-2}
Some dimensionless modules used in the discussion	$Pe_T = \frac{Lu_L^0 \rho_L C_{pL}}{\lambda} = 1.5$, where $u_L^0 = \frac{\varepsilon \bar{r}}{8\tau} \frac{2\sigma \cos\varphi}{\mu_L L}$ $Z = M_2 H_2 \frac{L}{\lambda} \frac{\beta_{12} P_{Gb}}{b_G R T_b^2} = 20.3$ $\Phi_M = k_G \frac{RT_b}{\beta_{12} P_{Gb}} L$; $Q_W = k_G \frac{L^2}{\lambda} \frac{Q_G}{b_G T_b}$

in a combination with the spline approximation technique used in this package allows us to obtain a solution even in those cases it is not simple.

3. Results and discussion

In numerical experiments, we calculate the steady-state distribution of liquid imbibition velocity, temperature, pressure, gas (or liquid) fraction, gas phase and liquid phase compositions along the catalyst particle. An example of the calculated profiles is presented in Fig. 1.

Studying the impact of the external wetting efficiency on the steady-state regimes of the particle, it was revealed that increasing the external wetting efficiency induces the liquid filling of the particle and causes almost isothermal conditions for the proceeding processes. Decreasing the external wetting efficiency results in formation of liquid–gas and dry zones inside the particle. This case is illustrated in Fig. 1. Curve 2 shows that while 0.34 external surface fraction of the left side of the slab is wetted, the right side of the slab is dry and there is a dry zone near this side. The fraction of liquid steadily decreases along the particle to the dry zone, since a more intense reaction and heat generation take place in gas-filled pores. Concentration profiles also show the reaction to be more rapid in the dry zone. The gas concentration gradient of the organic reactant is very small within the two-phase zone due to the vaporisation of α-methylstyrene from liquid phase, while it is great inside the dry zone. The vaporisation leads to the non-monotone temperature profile with a maximum value of the temperature inside the dry zone. The greatest temperature gradient is near the point of the interface between the dry and two-phase zones.

The dependence of the catalyst effectiveness, η, on the dimensionless catalytic activity modulus, Φ_M, for different values of the external wetting efficiency is presented in Fig. 2, where

$$\eta = \frac{\int_0^L (W_G(x_1, x_2, T, P_G) + W_L(C_1, C_2, T))\,dl}{(W_G(x_{1b}, x_{2b}, T_b, P_{Gb}) + W_L(C_{1b}, C_{2b}, T_b))L};$$

$$\Phi_M = k_G \frac{RT_b}{\beta_{12} P_{Gb}} L$$

The external wetting efficiency, α_{Lb}, has significant influence on the character of this dependence. The catalyst effectiveness decreases steadily for large values of α_{Lb} (e.g. for $\alpha_{Lb} = 0.62$ in Fig. 2). Under these conditions, the liquid flows throughout the particle at any catalytic activity, no formation of the dry zone is observed. The catalyst particle is almost isothermal due to the intense heat-transfer caused by the high values of the liquid hold up. The behaviour of the dependence η versus Φ_M is similar to the case of a single-phase exothermic reaction in a particle with external transport limitation.

The dependence under discussion becomes non-monotone when the external wetting efficiency decreases below 0.34 (curves 2–5 in Fig. 2). At the intermediate values of $\alpha_{Lb} =$ 0.2–0.34, the dependence η versus Φ_M is not simple (curves 3–5 in Fig. 2), i.e. multiplicity of the steady states exists for some region of Φ_M values. According to the above data (Fig. 1) the multiplicity of the steady states means that one of the steady states responds to the existence of the dry zone inside the particle with significant overheating. For the externally non-wetted particle the maximum value of catalyst effectiveness is significantly exceeds 1.0 due to the temperature rise inside the particle, which is induced by the reaction heat. It is worth noting that the results of the numerical experiments evidence that the catalyst effectiveness in partially-wetted steady state is significant but not so high in respect to that for the dry porous structure.

Thus, three different types of the catalyst particle steady states can be distinguished, when the particle constitutes:

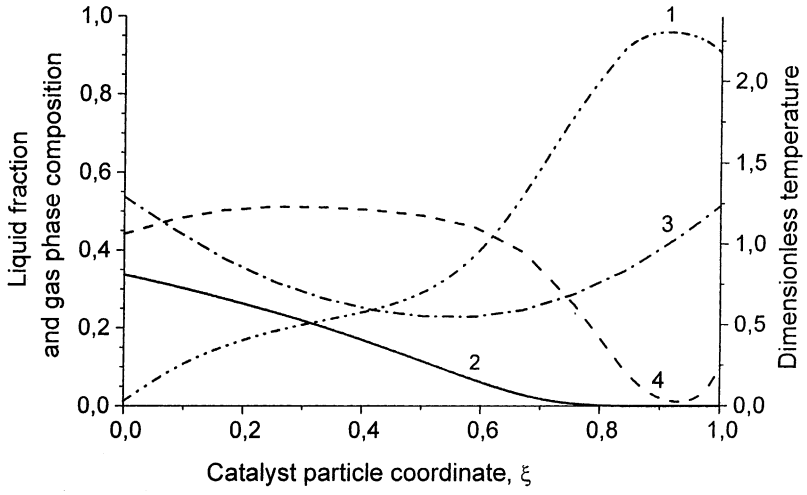

Fig. 1. The calculated profiles along the catalyst slab: curve 1, dimensionless temperature (θ); curve 2, liquid fraction (α_L); curve 3, mole fraction of H_2 in gas phase (x_1); curve 4, mole fraction of α-methylstyrene in gas phase (x_2). At $\Phi_M = 11$, upper state.

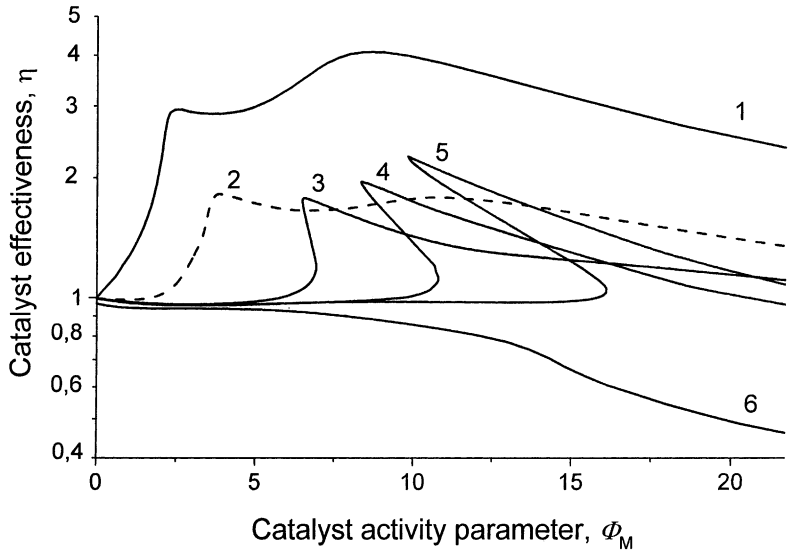

Fig. 2. The impact of the external wetting efficiency, α_{Lb}, and the catalyst activity parameter, Φ_M, on the catalyst effectiveness, η: curve 1, $\alpha_{Lb} = 0$; curve 2, $\alpha_{Lb} = 0.1$; curve 3, $\alpha_{Lb} = 0.2$; curve 4, $\alpha_{Lb} = 0.26$; curve 5, $\alpha_{Lb} = 0.34$; curve 6, $\alpha_{Lb} = 0.62$.

(A) practically non-wetted porous structure, where liquid contacts only external surface of the particle and is vaporised in the thin boundary layer (curve 1 in Fig. 2);
(B) completely liquid-filled porous structure, where liquid is filtered through the particle (the curve 6 and the "lower" branches of the curves 2–5 in Fig. 2);
(C) partially-wetted (and partially gas-filled) porous structure (the "upper" branches of the curves 2–5 in Fig. 2).

3.1. The effect of the reaction and phase transitions heat

Fig. 3 shows how multiplicity occurrence is connected with the formation of the dry zone inside the particle and how it depends on the interaction between the processes of heat generation by the exothermic reaction and heat consumption by the liquid vaporisation for the case of $\alpha_{Lb} = 0.26$. The dependence of the dry zone fraction on the heat generated by the reaction, $Q_W = k_G(L^2/\lambda)(Q_G/b_G T_b)$, reveals that there is no dry zone in the regime, which corresponds to the lower branch of the curve under discussion. The formation of the dry zone leads to its dramatic expansion due to the vaporisation, which is induced by the heat generated by the catalytic reaction within the dry zone. The process shifts to the upper partially-wetted regime. The heat consumption by the liquid evaporation, $Z = M_2 H_2(L/\lambda)(\beta_{12} P_{Gb}/b_G R T_b^2)$, also affects the possibility of the hot-spot ignition. The

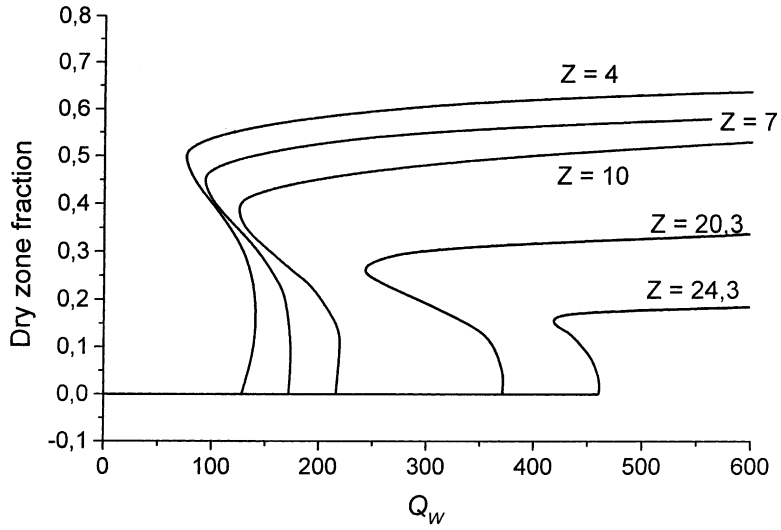

Fig. 3. The impact of the reaction heat, Q_W, and the effective heat of the liquid evaporation, Z, on the fraction of the dry zone inside the particle. For $\alpha_{Lb} = 0.26$.

higher the value of Z is, the more heat is to be generated by the reaction for the ignition of the hot-spot zone inside the particle. It is worth noting that the dry zone fraction decreases significantly, as the evaporation heat increases.

3.2. The effect of the wetting parameters on the multiplicity of the steady states

It was pointed out that at some range of the external wetting efficiency values the multiplicity area of the stationary states exists. The imbibition processes seem to be important for the origination of the above mentioned multiplicity. The wetting angle (for the catalyst–liquid interface) is one of the parameters, which affects the imbibition velocity. Fig. 4 shows the impact of the wetting angle, φ, and the external wetting efficiency, α_{Lb}, on the multiplicity area range (i.e. the marginal values of the catalyst activity parameter, Φ_{M}, between which the multiplicity exists). The upper branch of the curves corresponds to the hot-spot ignition points, the lower branch corresponding to the extinction ones. There is the area of the multiplicity of the steady states between the branches.

The multiplicity area depends on the value of the external wetting efficiency, α_{Lb}, as well as on the values of Φ_{M} and φ. For low values of the external wetting efficiency ($\alpha_{\mathrm{Lb}} < 0.3$), a decrease in the wetting angle causes the expansion of the multiplicity area and shifts it to the higher values of Φ_{M}. However, further increase of α_{Lb} leads to the contraction of the discussed area. It is disappearing from the low values of the wetting angle. In this case, the large liquid hold up inhibits the dry zone formation. Thus, the wetting parameters affect a lot the range of multiplicity.

3.3. The impact of the thermal conductivity

Fig. 5 shows the dependence of the dimensionless overheating, $\theta|_{l=L}$, on the apparent liquid imbibition flow at the left partially-wetted side of the slab, $(\alpha_{\mathrm{Lb}} u_{\mathrm{L}})(u_{\mathrm{L}}^0)|_{l=0}$, where $u_{\mathrm{L}}^0 = (\varepsilon \bar{r}/8\tau)(2\sigma \cos\varphi/\mu_{\mathrm{L}} L)$. Overheating is determined as the temperature difference between the right side of the slab (which contacts with the gas flow only) and the bulk temperatures: $\theta|_{l=L} = (T|_{l=L} - T_{\mathrm{b}})E_{\mathrm{G}}/R(T_{\mathrm{b}})^2$. This dependence is considered for different values of $Pe_{\mathrm{T}} = Lu_{\mathrm{L}}^0 \rho_{\mathrm{L}} C_{p_{\mathrm{L}}}/\lambda$.

The theoretical shape of the discussed dependencies depicted in Fig. 5, are in good agreement with the experimental data reported in [4] (see dashed line in Fig. 5). At low values of the imbibition flow, the particle overheating slightly decreases. High temperature at the right side of the catalyst particle indicates that a dry zone inside the particle exists. The contraction of this zone induces slight temperature fall at the dry right side of the particle until the imbibition flow becomes sufficient to wet the right side of the particle. The higher the value of parameter Pe_{T} is, the less liquid flow induces the filling the particle with the liquid and causes the dramatic fall of the temperature at the right (dry) side of the particle.

The obtained data evidence that the imbibition of liquid plays an extinction role in the multiphase process if the imbibition velocity is high. The extinction is more effective when the heat conductivity is rather small in comparison to the heat capacity of the liquid phase (high values of Pe_{T}).

This may indicate that at low values of heat conductivity, the temperature gradient near the hot-spot boundary is large and the catalytic reaction (i.e. heat generation) proceeds mostly in the hot-spot zone. The imbibing liquid is cold

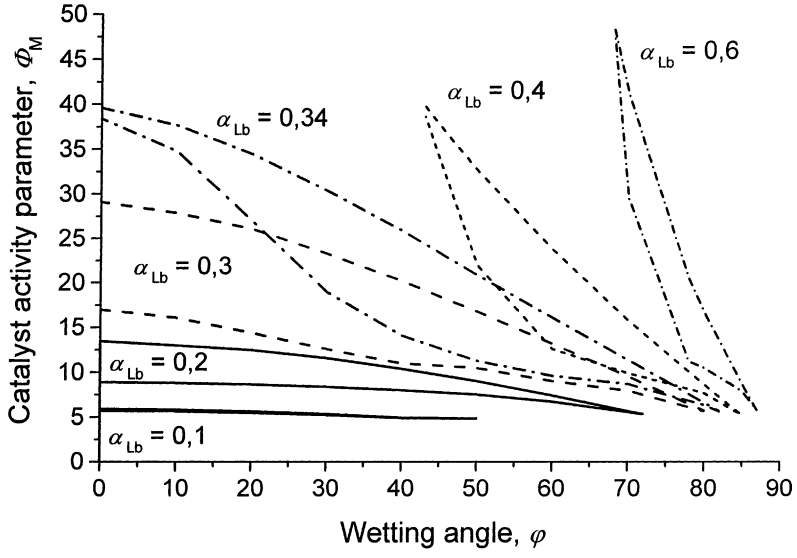

Fig. 4. The impact of the external wetting efficiency, α_{Lb}, the wetting angle, φ, and the catalyst activity parameter, Φ_{M}, on the multiplicity of the steady states. The dry zone exists in the region above the lower branches of the curves. The totally wetted state of the catalyst slab exists in the region below the upper branches of the curves. The multiplicity exists between the branches.

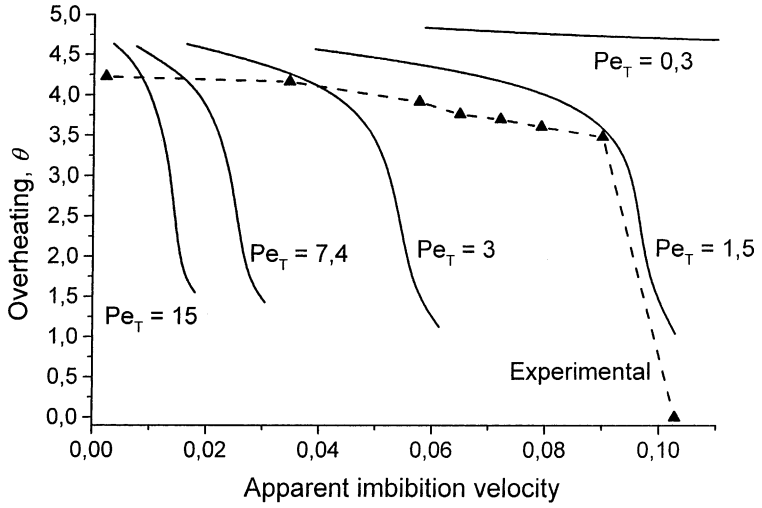

Fig. 5. The impact of the apparent liquid imbibition flow and Pe_T on the dimensionless overheating of the right side of the catalyst particle. At $\Phi_M = 45$. Experimental data (dashed line) are taken from [4].

when it comes to the hot-spot zone. Thus, the energy consumption for the heating of the coming liquid flow is significant and may cause the extinction of the catalytic process. On the other hand, at high values of heat conductivity, the hot-spot zone is diffuse, i.e. the temperature gradient from the "cold" liquid-filled zone to the dry one is less. The liquid flow is heated gradually during its way from the "cold" boundary of the particle. Thus, the extinction role of liquid imbibition is not so pronounced at high values of the heat conductivity.

4. Conclusions

The numerical study of the multiphase processes on a partially-wetted porous catalyst particle in the conditions of the exothermic catalytic reaction, species diffusion, phase transitions, and capillary phenomena interaction shows the following results:

1. Three different types of steady states of the catalyst particle can be distinguished, when the particle constitutes: (i) practically non-wetted porous structure, where liquid contacts only external surface of the particle and is vaporised in the thin boundary layer; (ii) completely liquid-filled porous structure, where liquid is filtered through the particle; (iii) partially-wetted (and partially gas-filled) porous structure.
2. The ignition of the hot-spot inside the particle is closely related to the dry zone formation inside the particle. The dry zone formation leads to its dramatic expansion due to the vaporisation, which is induced by the heat generated by the catalytic reaction within the dry zone and shifts the process to the partially-wetted regime.
3. The wetting parameters significantly affect the range of multiplicity. For low values of the external wetting efficiency, decreasing the wetting angle causes the expansion of the multiplicity region and shifts it to the higher values of Φ_M. However, increase in external wetting efficiency leads to the contraction of the discussed region due to the impact of the capillary phenomena.
4. The extinction role of the liquid imbibition is more effective when the effective heat conductivity is small.

Acknowledgements

This research was supported by RFBR Grant no. 99-01-00035.

References

[1] G.A. Funk, M.P. Harold, K.M. Ng, Experimental study of reaction in a partially wetted catalytic pellet, AIChE J. 37 (1991) 202–214.
[2] D.N. Kim, Y.G. Kim, An experimental study of multiple steady states in a porous catalyst due to phase transition, J. Chem. Eng. Jpn. 14 (1981) 311–317.
[3] P.C. Watson, M.P. Harold, Rate enhancement and multiplicity in a partially wetted and filled pellet: experimental study, AIChE J. 40 (1994) 97–111.
[4] M.G. Slin'ko, V.A. Kirillov, A.V. Kulikov, N.A. Kuzin, A.B. Shigarov, Thermal states of a partial wetted catalyst pellet in hydrocarbon hydrogenation, Doklady Chem. Tech. 373-375 (2000) 27–29.
[5] D.N. Kim, Y.G. Kim, Simulation of multiple steady states in a porous catalyst due to phase transition, J. Chem. Eng. Jpn. 14 (1981) 318–322.
[6] D.N. Jaguste, S.K. Bhatia, Partial internal wetting of catalyst particles: hysteresis effects, AIChE J. 37 (1991) 650–660.
[7] P.L. Mills, M.P. Dudukovich, A dual-series solution for the effectiveness factor of partially wetted catalysts in tricle-bed reactors, Ind. Eng. Chem. Fundam. 18 (1979) 139–149.

[8] I.V. Yentekakis, C.G. Vayenas, Effectiveness factors for reaction between volatile and non-volatile components in partially wetted catalysts, Chem. Eng. Sci. 42 (1987) 1323–1332.
[9] M.P. Harold, P.C. Watson, Bimolecular exothermic reaction with vaporisation in the half-wetted slab catalyst, Chem. Eng. Sci. 48 (1993) 981–1004.
[10] M.P. Harold, in: E.R. Becker, C.J. Pereira (Eds.), Computer-Aided Design of Catalysts, Marcel-Dekker, New York, 1991 (Chapter 11).
[11] M.G. Slin'ko, V.A. Kirillov, I.A. Mikhailova, S.I. Fadeev, Mathematical model of the gas–liquid–solid reaction on porous catalyst pellet, Doklady RAN 376 (2001) 219–223 (in Russian).
[12] L.D. Landau, Y.M. Lifshits, Statistical Physics, Nauka, Moscow, 1964, p. 568 (in Russian).
[13] E.A. Mason, A.P. Malinauskas, Gas Transport in Porous Media: The Dusty Gas Model, Chem. Eng. Monographs 17, Elsevier, Amsterdam, 1983.
[14] R. Krishna, G.L. Standart, Mass and energy transfer in multicomponent systems, Chem. Eng. Commun. 3 (1979) 201.
[15] L.I. Kheifets, A.V. Neimark, Multiphase Processes in the Porous Media, Khimiya, Moscow, 1982, p. 320 (in Russian).
[16] G.A. Hugmark, Mass and heat transfer from rigid spheres, AIChE J. 13 (1967) 1219.
[17] S.I. Fadeev, Organization of numerical experiment for investigation of non-linear boundary value problems by the method of continuation of solution with respect to parameter, Sib. J. Diff. Eq. 1 (1998) 321–350.